Unsteady fronts in an autocatalytic system

By N. J. Balmforth[1], R. V. Craster[2] & S. J. A. Malham[2]

[1]*Scripps Institution of Oceanography, University of California at San Diego, La Jolla, CA 92093, U.S.A.*

[2]*Department of Mathematics, Imperial College of Science, Technology and Medicine, London, SW7 2BZ, U.K.*

Travelling waves in a model for autocatalytic reactions have, for some parameter regimes, been suggested to have oscillatory instabilities. This instability is confirmed by various methods, including linear stability analysis (exploiting Evans' function) and direct numerical simulations. The front instability sets in when the order of the reaction, m, exceeds some threshold, $m_c(\tau)$, that depends on the inverse of the Lewis number, τ. The stability boundary, $m = m_c(\tau)$, is found numerically for m order one. In the limit $m \gg 1$ (in which the system becomes similar to combustion systems with Arrhenius kinetics), the method of matched asymptotic expansions is employed to find the asymptotic front speed and show that $m_c \sim (\tau - 1)^{-1}$ as $\tau \to 1$. Just beyond the stability boundary, the unstable rocking of the front saturates supercritically. If the order is increased still further, period doubling bifurcations occur, and, for small τ there is a transition to chaos through intermittency after the disappearance of a period-4 orbit.

1. Introduction

Many reaction-diffusion systems create coherent, localized structures that take the form of fronts separating distinct equilibrium phases. In many situations, the fronts propagate uniformly into one of the phases, but this is not always the case. For some systems, the steadily propagating fronts lose stability and as a result, the front advances in an oscillatory or even chaotic fashion (*e.g.* Bayliss & Matkowsky 1990; Shkadinskii *et al.* 1973; Ikeda & Mimura 1993; Mimura & Nishiura 1989; Elezgaray & Arneodo 1991).

Here, our interest is on the front dynamics in a particular autocatalytic reaction-diffusion system. For this system, Metcalf *et al.* (1994) have recently suggested that advancing fronts of the autocatalyst, $u(x,t)$, lose stability and begin rocking back and forth as they eat into the reactant, $v(x,t)$. They observed this phenomena in numerical solutions of the reaction-diffusion system for large reaction orders, m (the reaction terms are of the form $\pm u^m v$). In this limit there are some similarities with systems used in combustion theory.

In combustion theory the reaction terms have the exponential, Arrhenius behaviour and front instabilities have also been observed to occur in these systems as one increases the activation energy (Shkadinskii *et al.* 1973; Aldushin *et al.* 1975; Bayliss *et al.* 1989; Bayliss & Matkowsky 1990). Careful numerical simulations

(by the latter authors) demonstrate that the oscillatory solutions subsequently undergo further bifurcations to what appear to be chaotically propagating fronts.

Here we describe a thorough study of both the stability and transition behaviour of the front solutions arising in the autocatalytic system. The formulation of this system is mapped out in section 2, and the steady fronts themselves are described in section 3.

To explore front stability, we solve the linear stability problem in detail (section 4). In order to account for the infinite domain that the problem is ideally set in, we exploit Nyquist techniques via an Evans function (Evans 1975; Appendix A). This verifies that instability occurs when $m > m_c(\tau)$, a critical value that depends upon τ, the inverse of the Lewis number (the ratio of the reactant's diffusivity to that of the autocatalyst). As an addendum to Appendix A, we repeat the Nyquist calculation for combustion systems with Arrhenius kinetics, since numerical computations of the stability boundary appear not to have been given in the past.

In the combustion problem, advantage is often taken of an asymptotic analysis of the system for large activation energy (Sivashinsky 1977). In this limit, the front becomes very narrow and a matched asymptotic expansion facilitates the analytical calculation of the front speed and stability. This approach is paralleled in the limit of high reaction order, $m \gg 1$ in section 5 and Appendix B. As for the combustion system, we uncover the asymptotic speed of the front and the large-order location of the stability boundary.

Once we have mapped out the stability boundary $m_c(\tau)$ we solve the partial differential equations numerically and study the nonlinear dynamics of the front instability (section 6). We catalogue various bifurcations that eventually lead to what we interpret to be chaotic states.

Lastly, before we enter into the discussion of the problem, we should point out that large values of m are perhaps of less direct physical interest in autocatalysis; few reactions have order higher than 3. This does not mean that our study has little physical relevance. In fact, as will become apparent in the course of our study and will be remarked on in more detail in the concluding section, the autocatalytic problem is an exemplary one. It contains the simplest possible nonlinear terms that lead to an extreme sensitivity of the reaction rate to one of the components (auto-catalyst in the present context – at least for large m). It is essentially this extreme sensitivity that leads to front oscillations, and so our discussion bears upon any system with this physical property. In other words, the system studied here provides an ideal vehicle to investigate such front instabilities; this is as the nonlinear reaction terms are of such a simple type. The content of our study thus extends to far more general situations than merely a high-order auto-catalytic reaction.

2. Formulation

We consider autocatalytic reactions involving two diffusing chemicals in one spatial dimension. The autocatalyst and reactant are denoted by $u(x,t)$ and $v(x,t)$ respectively. Reaction terms of the form, $\pm u^m v$, are adopted where the reaction order, m is unspecified and treated as a parameter (this arises from

a physical model in which the autocatalyst U and reactant V combine in the proportion $U + mV$ to produce $(m+1)U$).

In non-dimensional coordinates, the underlying coupled equations are:

$$u_t = u_{xx} + vf(u) \tag{2.1}$$

and

$$v_t = \tau v_{xx} - vf(u), \tag{2.2}$$

where

$$f(u) = \begin{cases} u^m, & u \geq 0, \\ 0, & u < 0 \end{cases} \tag{2.3}$$

and τ is the inverse of the Lewis number (the ratio of diffusion rates). The range $\tau < 1$ is considered in detail within this paper. In addition we deal with $m \geq 2$, with m not necessarily integer.

For the boundary conditions and initial values, we take the following: The equations (2.1,2.2) are solved either on an infinite domain, or a semi-infinite one. The infinite domain is used to construct the form of the travelling fronts. In this case, we apply the conditions,

$$u(x,t) \to 1,\ v(x,t) \to 0 \text{ as } x \to -\infty \text{ and } u(x,t) \to 0,\ v(x,t) \to 1 \text{ as } x \to \infty. \tag{2.4}$$

We consider only steady solutions and their stability on the infinite domain.

For semi-infinite domains, $[0, \infty)$, we impose

$$u(0,t) = 1,\ v_x(0,t) = 0 \qquad \text{and} \qquad u(x,t) \to 0,\ v(x,t) \to 1 \text{ as } x \to \infty. \tag{2.5}$$

In these settings the initial-value problem is solved and we begin with

$$u(x,0) = e^{-x} \qquad \text{and} \qquad v(x,0) = 1. \tag{2.6}$$

In order to solve the PDE numerically in this initial-value problem, we replace the semi-infinite region by a long, finite domain and impose the right-hand boundary conditions at $x = L$. This approximation to the semi-infinite region remains accurate provided the front stays well away from the right-hand edge of the computational domain. In our numerical work, once the travelling wave solution has developed, we utilise a moving coordinate frame to try to minimize any such problems; this is described further in section 6a.

For smooth initial data the existence of unique global classical solutions for all $\tau > 0$ follows from Larrouturou (1988). This proof of existence utilizes the usual parabolic maximum principles which indicate that $u(x,t) \geq 0$ and $0 \leq v(x,t) \leq 1$. The positivity of $u(x,t)$ allows us to replace $f(u)$ by u^m, which we will do henceforth.

An important feature of the initial-value problem in (2.5)–(2.6) is that we can show (by adapting the techniques of Malham & Xin 1998; Appendix C) that, provided the initial conditions on $u(x,t)$ and $1 - v(x,t)$ decay exponentially with x, then they remain exponentially decaying for all time. Thus we may discount solutions such as algebraically decaying fronts (*cf.* Metcalf *et al.* 1994), and concentrate solely on exponentially decaying ones. Moreover, any relevant frontal instabilities must also decay exponentially, which allows us to use Evans functions (Appendix A).

3. Frontal solutions

As indicated by Metcalf *et al.* (1994), the autocatalytic equations (2.1,2.2) have solutions that take the form of travelling front solutions. For small m, these emerge as solutions to the PDE when the initial state of the system consists of a layer of the autocatalyst near the boundary at $x = 0$. This layer of autocatalyst subsequently expands into the reactant-rich region, and its leading edge converges to a steadily propagating front solution. For larger m much the same happens, save that the front propagates unsteadily.

To compute steadily propagating front equilibria, we introduce the moving coordinate frame, $\xi = x - ct$, and set $u(x,t) = U(\xi)$ and $v(x,t) = V(\xi)$. Then the coupled equations become

$$U_{\xi\xi} + U^m V = -cU_\xi, \quad \tau V_{\xi\xi} - U^m V = -cV_\xi. \tag{3.1}$$

Billingham & Needham (1991) show the existence of frontal solutions to these equations for $m = 2$; this proof can be extended to general m greater than 2. This proof establishes that there exists a unique front solution if and only if c is greater than a minimum value $c_\star(m,\tau)$. All of these fronts, bar the one travelling at speed $c = c_\star$ decay algebraically as $\xi \to \infty$ and are therefore ruled out in the initial value problem by previous arguments. The front with $c = c_\star$ decays exponentially and is the only one of interest here. Thus there is a trivial frontal selection criterion in this problem, unlike that for the Fisher equation (Langer 1980).

Note that, using methods based on those in Berestycki *et al.* (1985), we may place a lower bound the front speed:

$$c_\star \geq \sqrt{\frac{2}{(m+1)(m+2)}}. \tag{3.2}$$

This follows from the inequalities

$$0 \leq U, V \leq 1, \qquad -c \leq U' \leq 0, \qquad 0 \leq V' \leq \frac{c}{\tau}, \tag{3.3}$$

$$\frac{1}{\tau}(1-U) \leq V \leq 1 - U, \quad \text{if} \quad \tau \geq 1, \tag{3.4}$$

$$1 - U \leq V \leq \frac{1}{\tau}(1-U), \quad \text{if} \quad 0 < \tau \leq 1, \tag{3.5}$$

and various integral relations following from the front equations.

To find the form of the front by numerical means, we use either a Newton-Raphson-Kantorovich algorithm (Cash & Singhal 1982), or a shooting scheme. To model the infinite domain, we define a grid centred on an initial approximation to the front, then match the solution onto exponentially decaying tails at locations sufficiently far from the front that the amplitudes of U and V are close to their asymptotic ($\xi \to \pm\infty$) values. The numerical schemes then converge to the front shape and provide the front speed c as an eigenvalue.

Some numerical results are shown in figure 1, which shows a selection of front shapes, and in figure 2, which shows the front speed as a function of the parameters m and τ. Note that, as we increase m, the front associated with the reactant v steepens, whilst the gradient of the autocatalyst u decreases. This is a

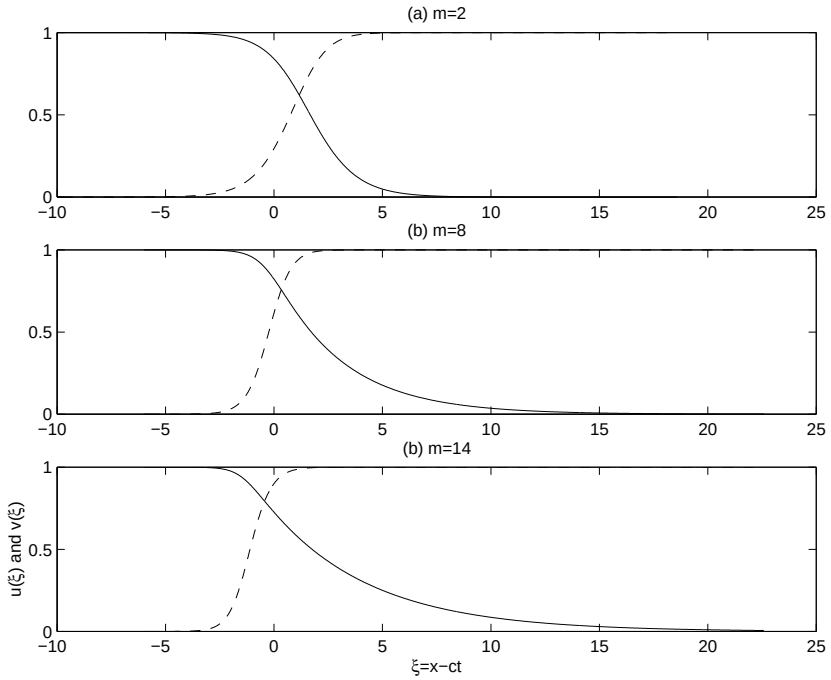

Figure 1. Front solutions for $\tau = 0.1$. The solid curve shows $U(\xi) = U(x - ct)$ and the dashed curves shows $V(\xi) = V(x - ct)$.

prelude to instability: the large gradient of reactant needs sufficient autocatalyst to sustain the required reaction rate. Any reduction in the autocatalyst at the reaction front (that is a deceleration of the front of $u(x,t)$) may eventually lead to an unbalanceable drop in the reactant gradient. The extra fuel then accelerates the production of the autocatalyst and drives the front of $u(x,t)$ forward. If this overshoots the equilibrium position, then the reactant rapidly combines with the autocatalyst and its gradient steepens beyond its equilibrium value. The reduced reactant concentration then lowers the reaction rate and the front of autocatalyst decelerates behind the equilibrium front. Provided the phases of the various steps are just right, the oscillation of the front of autocatalyst grows unstably. That is, a Hopf bifurcation occurs that sets the front into oscillatory motion.

4. Linear stability results

According to the results of Metcalf *et al.* (1994), for larger values of m, the fronts appear to lose stability and begin to rock back and forth as they propagate. To explore this issue further, we consider the linear stability problem for the fronts. In the frame of reference of the front, the stability problem is simply a differential eigenvalue problem with spatially varying coefficients.

We use two methods to determine the stability of the front solutions. The first is a simple algorithm: a Newton-Raphson-Kantorovich relaxation scheme that converges to an eigenvalue given an initially close guess. Again, the infinite domain is replaced by a finite one centred at the front, and asymptotic tails are patched onto the linear perturbations to provide boundary conditions. This fur-

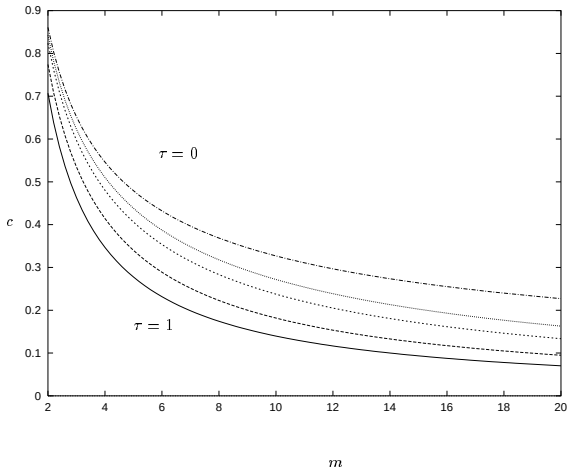

Figure 2. Front speed as a function of m for various values of τ. The particular values of τ shown are 0.0, 0.1, 0.2, 0.5 and 1.

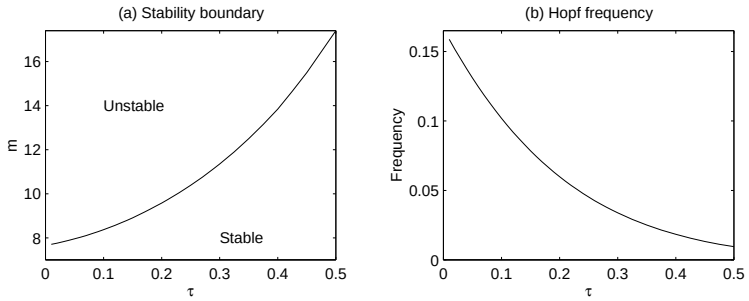

Figure 3. (a) Stability boundary, $m = m_c(\tau)$, and (b) Hopf frequency.

nishes eigenfunctions and the stability eigenvalues, but gives no guarantee that the most unstable mode has been located. The second method, however, gives precise information on the threshold of instability. This is the Nyquist method developed by Evans (1975) for pulses in nerve axon equations. By locating the zeros of a complex analytic function, the presence of unstable modes may be detected. The details are described in Appendix A. (There we also give the stability boundary for combustion systems with Arrhenius kinetics, both for comparative purposes and since this has not been computed in the past as far as we are aware.)

Both methods predict that the fronts lose stability for $m > m_c(\tau)$; this stability boundary, $m = m_c(\tau)$, is displayed in figure 3. Along this boundary there is a Hopf bifurcation that sets the front into motion; the oscillation (Hopf) frequency is also displayed in the figure.

An unstable eigenfunction for $m = 9$ and $\tau = 0.1$ is shown in figure 4. Note the relatively slow decay of the amplitude of the perturbation in $u(x,t)$ behind the front. This is significant of a "wake" that develops behind the oscillating front, and is evident in later figures that display numerical solutions to the full partial differential equations.

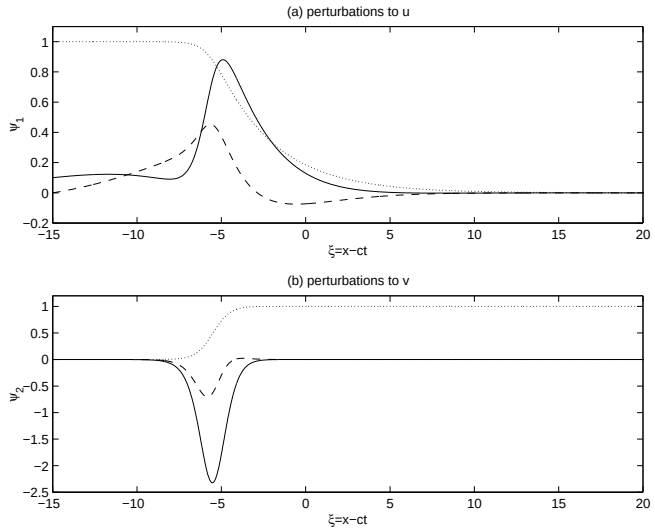

Figure 4. Unstable eigenfunction for $m = 9$ and $\tau = 0.1$. The solid lines show the real parts, and the dashed lines the imaginary parts, of the perturbations, ψ_1 and ψ_2, to u and v respectively. The dotted lines show the front. The eigenvalue $\lambda = (0.017, 0.094)$.

5. Matched asymptotic expansion

In the combustion problem with Arrhenius kinetics, analytical inroads into the frontal stability problem can be furnished by a matched asymptotic expansion in the limit of large activation energy (Fife 1980; Sivashinsky 1977). For our autocatalytic problem, there is an analogous development when $m \gg 1$. In fact, in this analytically tractable limit, our autocatalytic system becomes identical to the limiting form of the combustion problem. We indicate how this is realized in Appendix B, and we quote the results in this section.

The matched asymptotic expansion can be used both to construct the front solutions, and to determine their stability. The construction of the fronts can be performed for arbitrary Lewis number and leads to the asymptotic value of the front speed:

$$c \sim \sqrt{\frac{2}{m^2\tau}}. \tag{5.1}$$

This approximation is compared with numerical computations in figure 5.

For linear stability, the matched asymptotic expansion requires that one takes two solvability conditions. The first is that, at leading order, we must adopt $\tau = 1$, that is, we must expand about a Lewis number of unity. This is equivalent to the statement that for $\tau \to 1$, $m_c \to \infty$. The second solvability condition provides an explicit value for the order m^{-1} correction to the Lewis number; that is, $1 - \tau$. This generates a more refined estimate of the location of the stability boundary:

$$m_c \sim \frac{10.9282}{1-\tau}. \tag{5.2}$$

Moreover, the Hopf frequency is given by

$$\omega \sim 1.2712 m_c^{-2} \equiv 0.106(1-\tau)^2 \tag{5.3}$$

The asymptotic form of the stability boundary lies at too high a value of m_c

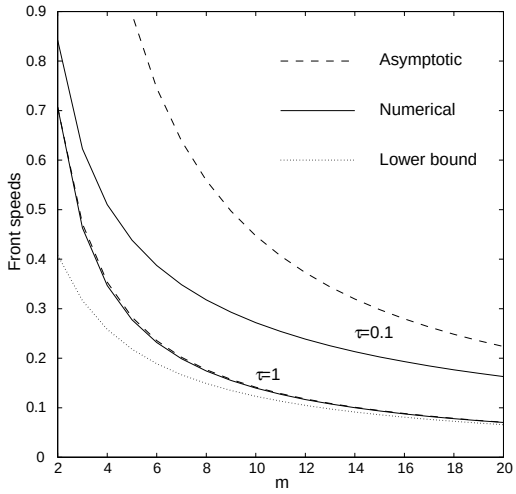

Figure 5. Numerically computed front speeds (solid lines) compared to asymptotic estimates given by (5.1) for large m (dashed lines). Shown are the speeds for $\tau = 0.1$ and $\tau = 1$. The lower bound given in (3.2) is also drawn as the dotted line.

and τ in order to attempt a serious comparison with numerical results. However, the main point is that the matched asymptotic expansion reveals that the front instability we have detected near $\tau = 0$ for smaller m_c continues upto $\tau = 1$. Moreover, it indicates that in the large m limit, the autocatalytic system and the combustion theories with Arrhenius kinetics are completely analogous.

The asymptotic theory also offers us insight into the weakly nonlinear dynamics of the instability (Matkowsky & Sivashinsky 1978), and into the two-dimensional, frontal instability problem (Sivashinsky 1977). In particular, in higher dimensions, nonplanar instabilities may appear for $\tau > 1$. This has been pursued recently by Hórvath *et al.* (1993) and Malevanets *et al.* (1995), see also Appendix D.

6. Numerical experiments

(*a*) *Computational details; moving into a translating frame*

The stability analysis confirms the front instability found by Metcalf *et al.* (1994). In this section we explore this instability and its consequences in more detail. We go about this by solving the PDEs numerically using two independent numerical schemes. One is based upon a moving, adaptive grid formulation and the other uses finite element and collocation methods. Both are designed to solve systems of nonlinear PDEs and are comprehensively documented, together with test examples, in Keast & Muir (1991) and Blom & Zegeling (1994) respectively. In our computations, where the solutions are reliable, no difference could be discerned between the solutions generated by the different codes.

One major difficulty in solving the PDE for extensive periods of time is that the front moves with order one speed. Hence when solving the PDE on a finite domain the interesting part of the solution rapidly sweeps across the domain and impinges on the right-hand boundary. Moreover, this impact occurs too soon for us to build an accurate picture of the developing instability of the front. That is,

the front hits the right-hand edge of the computational domain before there is sufficient time to catalogue the bifurcation to instability and beyond.

To avoid this unappealing aspect of the initial-value problem we make the following argument (see also Bayliss *et al.* 1989). Shortly after the inception of the numerical experiment, the solution develops into a front and propagates into the centre of the computational domain; if m is sufficiently large, the advance of the front is unsteady as a result of the instability. However, once the front has advanced into the central regions, the effect of the boundary conditions at the edges of the finite domain become exponentially small (because the tails of the front, stable or unstable, decay exponentially). At that moment, therefore, we transform into a moving frame determined by either the speed of the equilibrium travelling front (and given by the calculations described above), or that speed plus a small correction to account for the drift induced by the front oscillations (determined empirically)†. In the moving frame, we apply the same boundary conditions. This corresponds to a peculiar physical situation in which the boundaries are uniformly translating in space with the equilibrium front speed or a modification of that speed. However, since the precise boundary conditions at this stage are not very important, the transformation into the moving frame does not influence the dynamics of the front instability; this remains localized to the front position. Thereafter, the front remains on average centred in the middle of the computational domain, and we may follow the evolution of the instability for substantially longer intervals. The plausibility of these arguments is bolstered by several computational checks.

(*b*) *Periodic states*

To study the nonlinear dynamics of the front instability, we focus on two particular pathways in parameter space. We fix either $\tau = 0.001$ or $\tau = 0.1$ and vary m. According to the stability analysis, the instability then sets in at $m = 7.65$ or $m \simeq 8.35$, respectively.

The evolution of the front position, $X(t)$, that we define as the location for which $u(X,t) = 1/2$, is shown in figure 6 for a set of computational runs with different values of m (and $\tau = 0.1$). For the smallest value of m, the front is stable and moves steadily into the centre of the domain where (at time $t = 320$) it becomes pinned as a result of suddenly shifting into the translating frame. In the other numerical experiments, the front is unstable, and the position becomes time-dependent.

At the front position, the reactant has concentration $Y(t) = v(X,t)$. This is shown in figure 7. The sudden change from the rest frame into the translating one is not apparent in this figure, illustrating how the change in the boundary conditions has an unimportant effect. (Also, choosing different instances in which to switch into the translating frame has no effect, nor does increasing the length of the domain.)

Just after the onset of instability, the front settles into a periodic rocking motion (figure 6(b)-(d) and 7(b)-(d)). A more detailed view of this oscillation is shown in figure 8, which shows the solution for $u(\xi,t)$ as a surface plot above the $(\xi,t)-$plane.

† Note that the empirical correction is invariably *negative*. Thus the unsteady fronts move more slowly than the unstable steady ones. This feature of the instability may prove important in some applications.

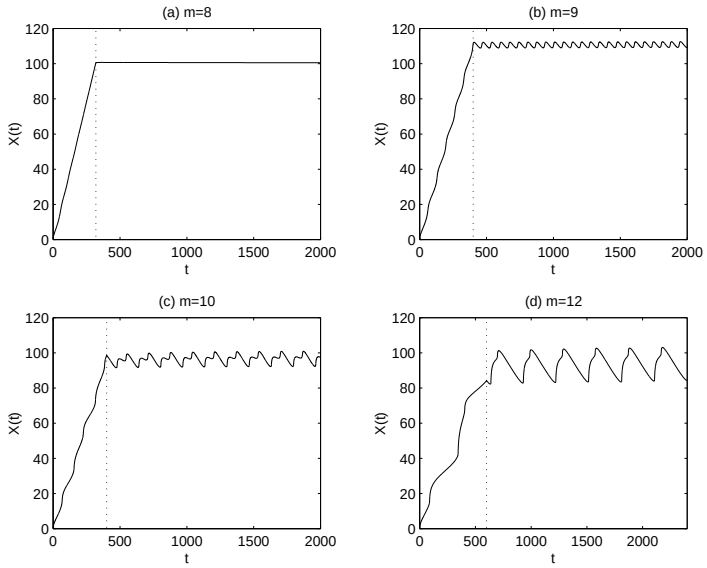

Figure 6. Front positions, $X(t)$. The vertical dotted lines indicate the time at which the computation suddenly switches into the moving frame. The frame speed is based on the equilibrium front speed. However, when the instability sets the front into unsteady motion, there is mean drift in the front position relative to the speed of the unstable equilibrium front; this is also taken into account in these experiments.

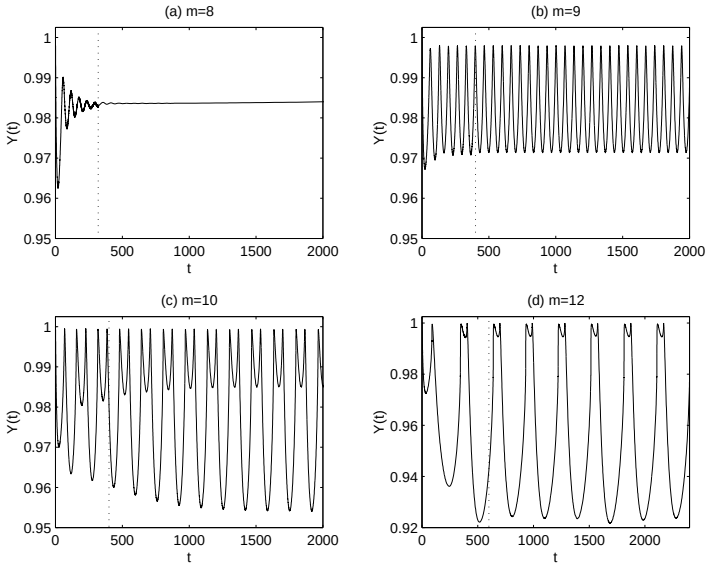

Figure 7. The value of the reactant, $Y(t) = v(X(t), t)$ at the front position, $X(t)$.

If we raise m further, the periodic motion of the front becomes more complicated. The rocking motion of the front can be represented by a simple limit cycle in the front position $X(t)$ just beyond the threshold of instability. As m is raised through about 8.49 for $\tau = 0.001$ or 9.59 for $\tau = 0.1$, this limit cycle loses stability in a period doubling bifurcation, leading to the doubly peaked character of the front oscillation (see figures 6 and 7). This is brought out in more detail

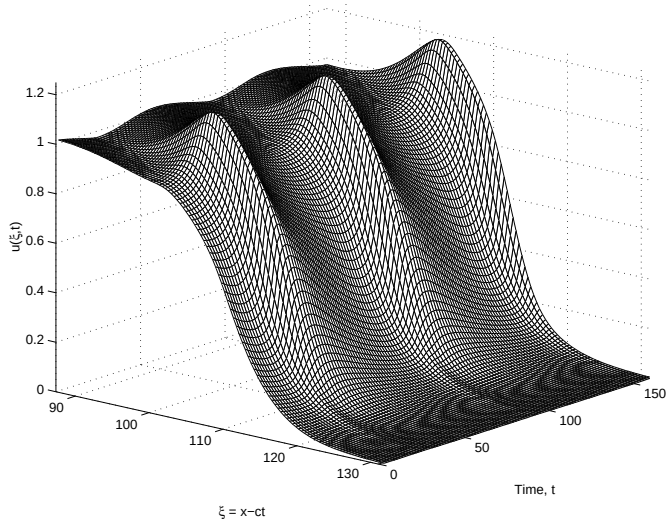

Figure 8. Oscillating front with $\tau = 0.1$ and $m = 9$. Shown is $u(\xi, t)$ for two periods of the oscillation as a surface plot above the $(\xi, t)-$plane.

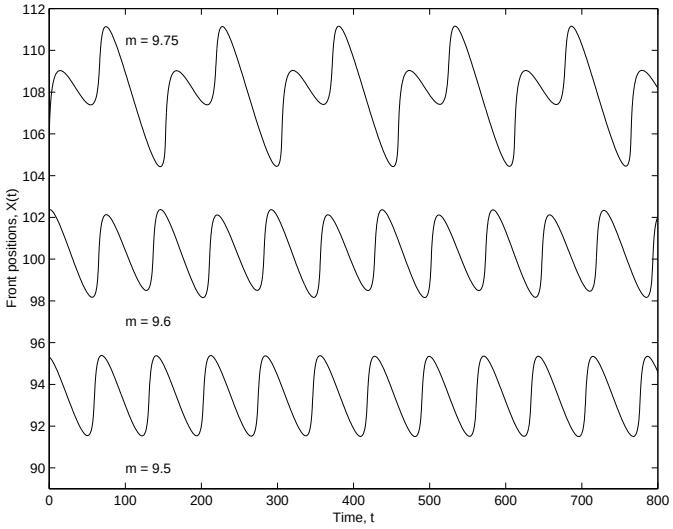

Figure 9. Time series of $X(t)$ near the period doubling point.

in the time series of $X(t)$ shown in figure 9, and the phase portraits of figure 10 that display the solutions projected onto the $Y - Y_x$ plane, where $Y_x = v_x(X, t)$ (we prefer Y and Y_x as coordinates for the phase portrait because it is not always possible to precisely subtract off the drift of periodic solutions, and, in fact, that procedure becomes ambiguous for the less regular states).

Bifurcation diagrams are shown in figure 11. This displays the excursion in $Y(t)$ during the limit cycle. Once the period has doubled, the two possible values of this quantity are shown. The smooth connections amongst the various branches and to the zero-amplitude (steady) states provides numerical evidence that the Hopf bifurcation and period doublings are supercritical. The supercriticality of the

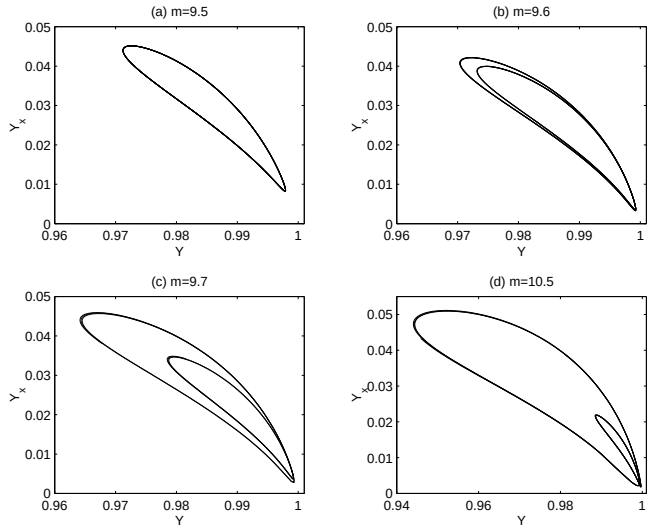

Figure 10. Limit cycles before and after period doubling. Shown are projections of the phase portraits onto the $(Y, Y_x)-$plane, where $Y = v(X,t)$ and $Y_x = v_x(X,t)$ and $X(t)$ is the front position.

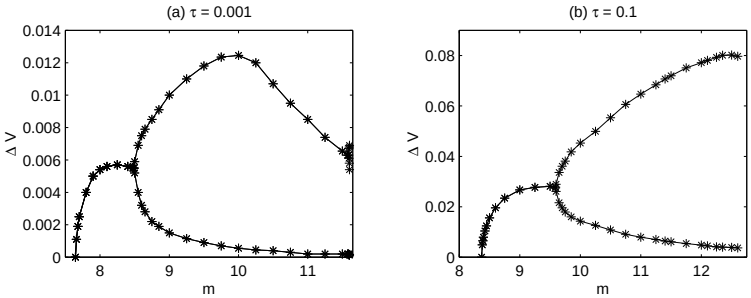

Figure 11. Bifurcation diagrams for (a) $\tau = 0.001$ and (b) $\tau = 0.1$. Shown is the excursion in $Y(t)$ during the limit cycle; the two (four) possible values of this excursion are shown after the period doubling bifurcations. The leftmost points indicate neutrally stable, steadily propagating fronts.

initial Hopf bifurcation is also confirmed by matched asymptotic analysis if one retains nonlinear terms and proceeds to higher order (Matkowsky & Sivashinsky 1978).

(*c*) *Chaotic states*

For the largest values of m shown in figure 11, the solutions become relatively difficult to compute accurately; the oscillations are now characterized by extremely sharp features in the autocatalyst concentration (see figure 12; *cf.* Metcalf *et al.* (1994)). The numerical codes have difficulty tracking the violent excursions and these numerical problems prevent us from continuing to much higher values of m, especially for the larger values of τ. Of the two routines utilized, the EPDCOL routine of Keast & Muir (1991) proved to be more robust, and converged more rapidly under these more arduous conditions. By performing some high accuracy computational runs, we were able to observe some further bifurcations to what we interpret to be chaotic states.

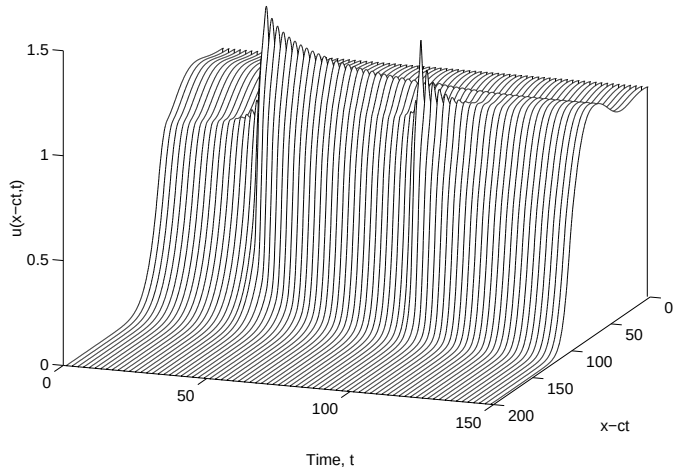

Figure 12. Oscillating front with $\tau = 0.1$ and $m = 12$. Shown is $u(\xi, t)$ over part of the cycle, as a plot above the $(\xi, t)-$plane.

For $\tau = 0.001$, the limit cycle again passes through a period doubling bifurcation at $m \simeq 11.59$ (figure 13; a similar bifurcation occurs for $\tau = 0.1$, but we have neither precisely located it in m, nor followed the subsequent behaviour in detail because of computational limitations). This is also shown in the bifurcation diagram of figure 11 by the cluster of points at the right-hand edge of the range in m. Shortly thereafter we observe temporally irregular states (figure 14). The two period doublings and the structure of the objects that exist for large m imply that the oscillating front has many of the hall marks of a system undergoing a period doubling cascade to chaos. However, a fine exploration of the solutions in the range $11.6 < m < 11.65$ indicates that this is not the actual route to chaos.

The actual transition appears to be of the Pomeau-Manneville intermittency variety. A telling time trace is shown in figure 15. This clearly reveals an intermittent period-4 oscillation (it appears to be period-2 because one of the original loops of the period-2 orbit has shrunk to a very tight loop and is not discernible in either the time traces or phase portraits at these values of m). Further evidence for this scenario is shown in figure 16 which shows return maps obtained from a Poincaré section taken at the minimal values of Y with $Y < 0.999$. Thus, the period-4 limit cycle disappears in a saddle-node bifurcation. What then remains is what we conjecture to be a strange attractor (though we have neither shown this rigorously, nor traced where the associated set of unstable periodic orbits may have originated).

The phase portraits and return maps in figures 13 and 16 both suggest that the attractor has a low dimension: the phase portraits show a relatively simple geometry and the return maps are reminiscent of the multi-leaved, almost one-dimensional maps typical of low-dimensional systems with a single positive Lyapunov exponent. Hence underlying the dynamics of the system in this regime is probably a low-order attractor. In any case, the familiar appearance of the phase portraits and maps give us confidence in our prediction of chaos.

As we continue to raise m, the front oscillations becomes wilder and wilder.

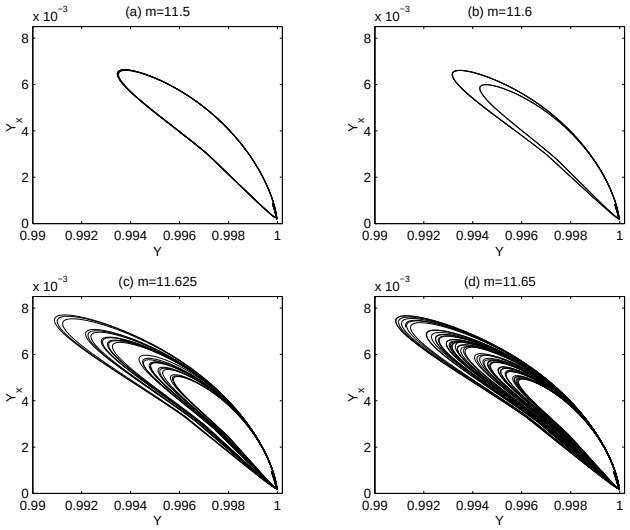

Figure 13. Limit cycles and presumably strange attractors. Shown are phase portraits projected onto the $(Y, Y_x)-$plane. In panel (a), the period-2 solution is shown for $m = 11.5$. In (b), the period-4 solution is shown at $m = 11.6$. Panels (c) and (d) show solutions that we interpret to be chaotic. Loops near $Y = 1$ and $Y_x = 0$ are barely discernible.

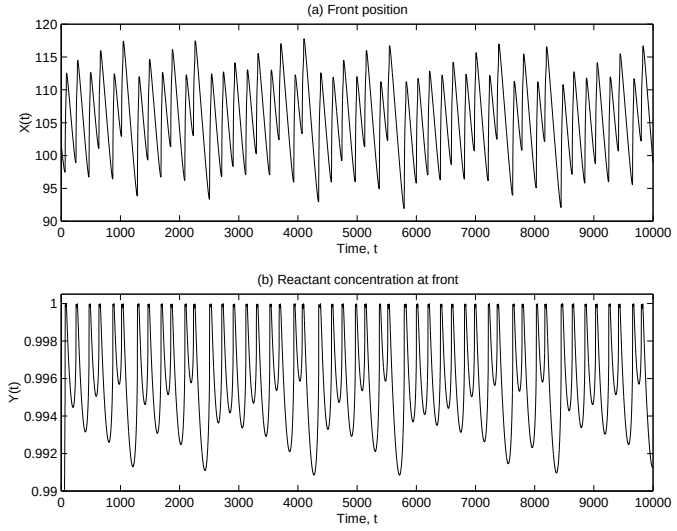

Figure 14. Presumably chaotic time trace at $m = 11.65$.

Unfortunately, numerical problems prevent us from continuing much beyond the transition to chaos. The solution at $m = 13$ is shown in figure 17. The attractor evidently covers a much larger region of phase space; this probably occurs through the intersection of the original chaotic set with a fixed point, but we have not made any effort to find this crisis.

Numerical problems are also encountered in the combustion problem with Arrhenius kinetics. The more accurate computations there suggest a transition to chaos which, for models with melting fronts, is also through intermittency (Bayliss & Matkowsky 1990). Combustion models without melting fronts (which are more

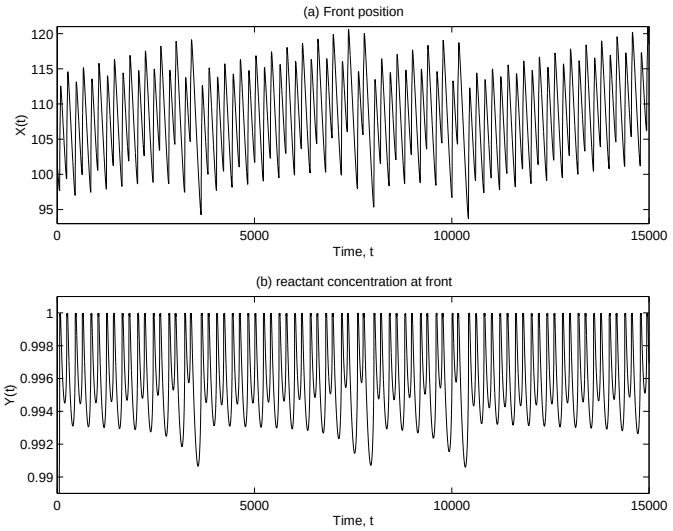

Figure 15. Intermittent time trace at $m = 11.605$.

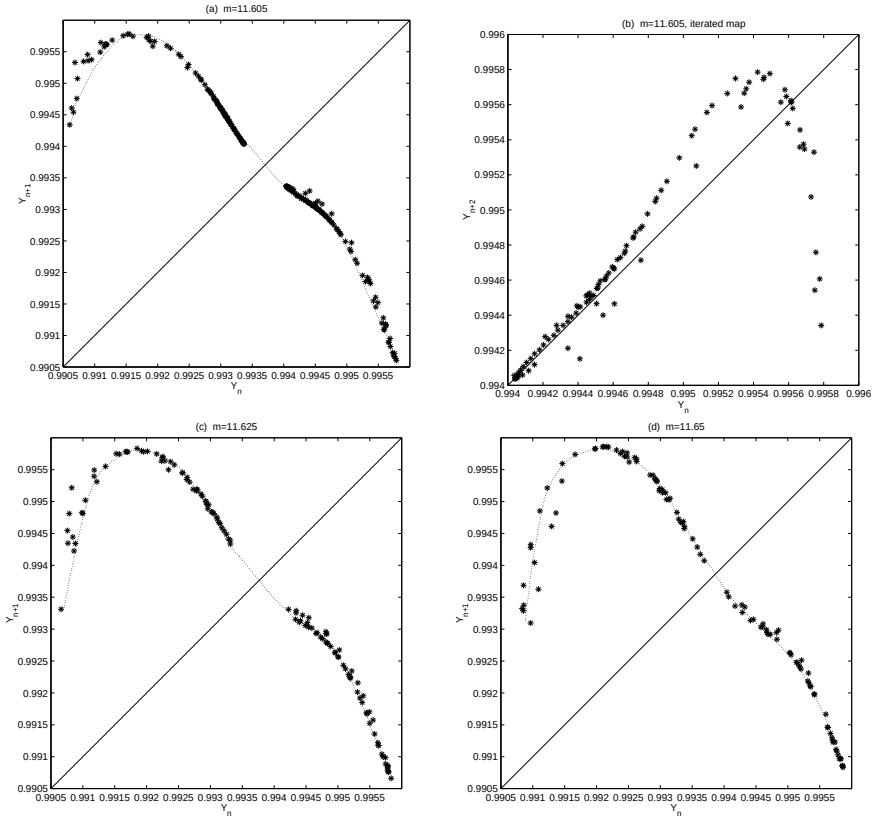

Figure 16. Panels (a), (c) and (d) show return maps at the Poincaré section taken at the minimal values of Y with $Y < 0.999$. Panel (b) is the twice-iterated map corresponding to (a). The dotted lines show curves fitted to the data. Transients from the initial conditions are not suppressed, which accounts for some of the outlying points.

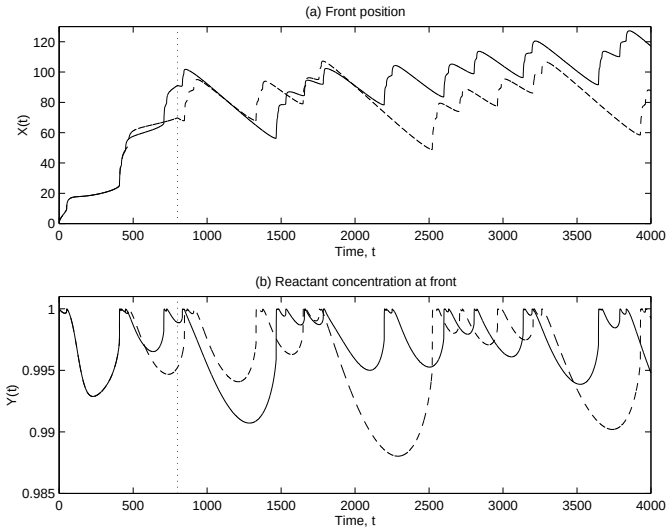

Figure 17. Evolution at $\tau = 0.001$ and $m = 13$. Two computational runs from slightly different initial conditions are shown.

directly analogous to our system), however, show period doubling cascades. None the less, the return maps of figure 16 suggest that it would probably only take a slight variation in the system to find a period doubling cascade here also.

Note that, even though the transition to chaos does not occur until $m \simeq 11.6$ for $\tau \simeq 0$, the initial, transient behaviour is fairly irregular even for lower m (as suggested by Metcalf *et al.* 1994). In some situations this may be more relevant than the ultimate attractor of the system.

7. Concluding remarks

This study confirms, and explores in depth, the existence and properties of the front instability suggested by the numerical experiments of Metcalf *et al.* (1994). We find this instability saturates supercritically just beyond the stability threshold, $m = m_c(\tau)$. Moreover, as we increase m further, the rocking of the front becomes more pronounced; two period doubling bifurcations later, the stable periodic oscillation of the front disappears, leaving what appears to be chaos. For larger m, the solutions are very erratic indeed, and substantial numerical problems preclude us following the solutions much further.

Another area explored by this study is the two-dimensional frontal stability problem, see Appendix D. It is known in the Arrhenius problem (*e.g.* Fife 1980) that fronts in two dimensions can have substantially different stability properties from their one-dimensional relations: the onset of instability for $\tau < 1$ arises at finite transverse wavenumber, and front corrugations arise for $\tau > 1$ (see also Hórvath *et al* 1993; Malevanets *et al* 1996). It is straightforward to extend the Nyquist theory (Evans function) to detect two-dimensional instabilities. We simply include the dependence on the new coordinate through the transverse wavenumber, k, in the stability equations, see Appendix D. Moreover, the Evans function can then be shown to depend upon the parameter k^2. Hence we may repeat the Nyquist plots for each k in turn to detect instability (we can further

exploit continuity in k^2 so that the calculation is not an open-ended one). The major result here is that for $\tau < 1$ the marginal stability boundaries are not substantially altered. For $\tau > 1$ we present various results extending previous work to arbitrary orders of autocatalysis.

In a different direction, the current work has demonstrated the close analogy between the power-law reaction terms at large order and Arrhenius kinetics with large activation energy. In these limits, our matched asymptotics reveal a common behaviour, though even at less extreme parameter settings, the systems have similarities. In fact, we can make some remarks of a more general nature concerning the kinds of nonlinear reaction terms that will lead to the frontal dynamics we have explored.

Basically, the key feature of the auto-catalytic and combustion systems that leads to the front oscillations is the extreme sensitivity of the reaction rate to one of the components (auto-catalyst in the one case, temperature in the other). We therefore conjecture that these front oscillations will appear in any two-component reaction-diffusion system provided the nonlinear reaction terms are of the form, $\pm F(u, v)$, with $F(u, v)$ a rapidly increasing nonlinear function of u. Indeed, if $F(u, v) = vf(u)$, then the stage is again set for a matched asymptotic expansion of the flavour of that in Appendix B, whatever the precise form of $f(u)$. This observation suggests that the content of our study extends to far more general situations than merely a high-order auto-catalytic reaction. This is somewhat reassuring since at present there appear to be few examples of such reactions with sufficiently high order to imply the possibility of front instability. Moreover, those that do exist appear to rely on some complicated, additional hydrodynamic interactions (Nagypal & Epstein 1983).

However, high-order autocatalytic reactions of the form $\pm u^m v$ arise as an approximation to multistep reactions. Alternatively one can explicitly account for the multiple components and treat several coupled reaction–diffusion equations. In this circumstance the reaction terms analogous to $\pm u^m v$ may not necessarily be of high order to create front instability. Hence there may be experimentally realizable multistep reactions for which frontal instabilities could be an issue. In this context, we remark that Solovyov *et al.* (1997) have recently observed complicated front oscillations in a multicomponent model of polymerization for which there are related experiments.

We close by suggesting some possible applications. As remarked by Metcalf *et al.* (1994), one of the drawbacks of Arrhenius kinetics is the so-called cold-boundary problem (which translates to the requirement that we cut off the reaction term artificially at some ignition temperature – see Appendix A). As a result it is not always clear whether the dynamics of the model represents a reaction-diffusion phenomenon or whether it arises directly as a result of the cut-off. Notably for $\tau > 1$ one cannot show that there are unique front solutions in the Arrhenius problem (Berestycki *et al* 1985). In fact Bonnet *et al.* (1993) suggest that there are multiple front solutions. We suspect that this multiplicity is entirely an artifact of the cut–off at the ignition temperature, since there are unique exponentially decaying fronts for all τ in the autocatalytic model. These technical problems and the similarities between the Arrhenius systems and our auto-catalytic model suggest the latter as a convenient alternative (Metcalf *et al.* 1994 cite references in which this alternative model has been used in combustion theory).

For a direct application of frontal instability, we require systems for which the reaction rate is extremely sensitive to one of the components. This criterion is satisfied in several situations. For example, the nuclear reactions that occur within stellar cores are characterized by rates that depend on a very high power of the temperature. Moreover, combustion waves are thought to occur in some of the more energetic phases of stellar evolution (supernovae, dwarf novae and helium flashes). We conjecture that frontal instability might be an important ingredient in the physics of these phenomena.

Acknowledgements: NJB thanks the Nuffield Foundation for an equipment grant. RVC thanks the EPSRC for providing support via an Advanced Fellowship.

Appendix A. Evans function and Nyquist plots

Evans functions provide information regarding the linear stability of steadily propagating, localized solutions. Although originated by Evans (1975) for impulses in models of nerve axons, the method has recently reached a wider audience (Pego and Weinstein 1992; Pego *et al.* 1993 and Alexander *et al.* 1990).) Indeed the approach is quite versatile and ideally suited to the purpose for which it is used here.

We first linearize the governing equation around the front solution, $U(x-ct)$ and $V(x-ct)$, by setting

$$u(x,t) = U(x-ct) + \psi_1(x-ct,t), \quad v(x,t) = V(x-ct) + \psi_2(x-ct,t). \tag{A 1}$$

The coupled evolution equations for the linear perturbations, ψ_1, ψ_2, are

$$\psi_{1t} = \psi_{1\xi\xi} + mU^{m-1}V\psi_1 + U^m\psi_2 + c\psi_{1\xi}, \tag{A 2}$$

$$\psi_{2t} = \tau\psi_{2\xi\xi} - mU^{m-1}V\psi_1 - U^m\psi_2 + c\psi_{2\xi}. \tag{A 3}$$

These relations are combined into the matrix equation,

$$\begin{pmatrix} \psi_{1t} \\ \psi_{2t} \end{pmatrix} = A \begin{pmatrix} \psi_1 \\ \psi_2 \end{pmatrix}, \tag{A 4}$$

where the matrix operator A is

$$A = \begin{pmatrix} \partial_\xi^2 + mU^{m-1}V + c\partial_\xi & U^m \\ -mU^{m-1}V & \tau\partial_\xi^2 - U^m + c\partial_\xi \end{pmatrix}. \tag{A 5}$$

The stability of the front is determined from the spectrum of the operator A. This spectrum consists of an discrete spectrum of isolated eigenvalues and a continuous spectrum. Because the front solution, U and V, has the asymptotic behaviour,

$$U \to 1,\ V \to 0 \text{ as } \xi \to -\infty, \tag{A 6}$$

$$U \to 0,\ V \to 1 \text{ as } \xi \to +\infty, \tag{A 7}$$

the location of the continuous spectrum on the spectral plane follows from considering the limits of the operator A:

$$A_\infty = \begin{pmatrix} \partial_\xi^2 + c\partial_\xi & 0 \\ 0 & \tau\partial_\xi^2 + c\partial_\xi \end{pmatrix}, \tag{A 8}$$

$$A_{-\infty} = \begin{pmatrix} \partial_\xi^2 + c\partial_\xi & 1 \\ 0 & \tau\partial_\xi^2 - 1 + c\partial_\xi \end{pmatrix}. \tag{A 9}$$

On introducing the exponential dependence, $\exp(\lambda t + i\alpha\xi)$, it follows that the continuous spectrum lies along the curves,

$$S_1^+ = \lambda : \lambda = -\alpha^2 + ci\alpha,\ S_2^+ = \lambda : \lambda = -\tau\alpha^2 + ci\alpha, \tag{A 10}$$

$$S_1^- = \lambda : \lambda = -\alpha^2 + ci\alpha,\ S_2^- = \lambda : \lambda = -\tau\alpha^2 + ci\alpha - 1, \tag{A 11}$$

for real α. These are all parabolic paths in the left half of the complex λ plane; all bar the last path touch the origin when $\alpha = 0$. The first (second) pair of curves correspond to solutions that decay to the right (left), but oscillate with finite amplitude as $\xi \to \infty$ ($\xi \to -\infty$). The dispersion relation of the linear perturbations possesses branch cuts along the curves of the continuous spectrum. However, since they lie in the left half plane, these cuts have no influence upon the transition to instability. (By Henry (1981), the essential spectrum, i.e. the spectrum not including any isolated eigenvalues of finite multiplicity, is contained within the union of the regions inside or on the curves S^+ and S^-.)

The transition to instability occurs when a discrete eigenvalue moves from the left half plane into the right half plane. The existence of such eigenvalues are determined via the Evans function $D(\lambda)$: If we let $\psi_j(\xi, t) = \Psi_j(\xi)e^{\lambda t}$, for $j = 1, 2$, then if λ is an eigenvalue of A with eigenfunction $\mathbf{\Psi}(\xi)$, then $\mathbf{\Psi}(\xi)$ must solve the system of differential equations,

$$\lambda\mathbf{\Psi}(\xi) = A\mathbf{\Psi}(\xi). \tag{A 12}$$

As $\xi \to \pm\infty$, this system reduces to the constant coefficient equations,

$$\lambda\mathbf{\Psi}(\xi) = A_\infty\mathbf{\Psi}(\xi), \quad \lambda\mathbf{\Psi}(\xi) = A_{-\infty}\mathbf{\Psi}(\xi). \tag{A 13}$$

These relations have solutions of the form $\exp(\mu_j^\pm\xi)$, for $j = 1 - 4$, where

$$\mu_{1,2}^+ = \frac{-c \pm (c^2 + 4\lambda)^{\frac{1}{2}}}{2}, \qquad \mu_{3,4}^+ = \frac{-c \pm (c^2 + 4\tau\lambda)^{\frac{1}{2}}}{2\tau}, \tag{A 14}$$

$$\mu_{1,2}^- = \frac{-c \pm (c^2 + 4\lambda)^{\frac{1}{2}}}{2}, \qquad \mu_{3,4}^- = \frac{-c \pm (c^2 + 4\tau(\lambda+1))^{\frac{1}{2}}}{2\tau}. \tag{A 15}$$

The μ_js characterize the growth or decay of the eigenfunctions at $\xi = \pm\infty$. The subscripts $1, 2$ in j are associated with the eigenfunction $\mathbf{\Psi_1}$ and $3, 4$ with $\mathbf{\Psi_2}$. In addition, we choose μ_2, μ_4 to be such that $\mathrm{Re}(\mu_j) > 0$. Thus, we identify a solution of (A 12) that decays as $\xi \to -\infty$ as

$$\mathbf{\Psi}^-(\xi) \sim \begin{pmatrix} \exp(\mu_2^-\xi) \\ \exp(\mu_4^-\xi) \end{pmatrix}. \tag{A 16}$$

When we integrate these solutions through the front position and onto $\xi \to +\infty$, we obtain

$$\mathbf{\Psi}^+(\xi) \sim \begin{pmatrix} d_1(\lambda)\exp(\mu_2^+\xi) \\ d_2(\lambda)\exp(\mu_4^+\xi) \end{pmatrix}. \tag{A 17}$$

The quantities $d_1(\lambda)$ and $d_2(\lambda)$ are sometimes loosely referred to as transmission coefficients. For solutions that decay exponentially as $\xi \to +\infty$, both $d_1(\lambda)$ and $d_2(\lambda)$ must vanish; then λ is an eigenvalue with eigenfunction $\mathbf{\Psi}^+(\xi)$.

Computationally we solve two complementary problems, one where

$$\mathbf{\Psi}^-(\xi) \sim (\exp(\mu_2^-\xi), 0)^T,$$

for which the transmission coefficients are $d_{1a}(\lambda), d_{2a}(\lambda)$, and the other where

$$\mathbf{\Psi}^-(\xi) \sim (0, \exp(\mu_4^-\xi))^T,$$

with transmission coefficients $d_{1b}(\lambda), d_{2b}(\lambda)$. Both initial-value problems are solved using a numerical scheme that avoids complications due to exponentially growing terms as $\xi \to +\infty$ (such schemes are discussed in Swinton and Elgin 1990, Pego *et al* 1993). The Evans function $D(\lambda)$ is then defined via the determinant,

$$D(\lambda) = d_{2a}(\lambda)d_{1b}(\lambda) - d_{2b}(\lambda)d_{1a}(\lambda). \qquad \text{(A 18)}$$

This defines an analytic function of λ whose zeros are the eigenvalues of (A 12).

The transitions to instability are clearly seen by drawing Nyquist plots. These are pictures of the locus of $D(\lambda)$ on the $(D_r, D_i)-$plane as λ varies along the imaginary axis; that is $D(iy)$ for $-\infty < y < \infty$. By the argument principle, the *integral* number of times this locus winds around the origin is equal to the number of unstable eigenmodes. One other point is that $D(\lambda) \to 1$ as $|\lambda| \to 1$; the Nyquist figures show the detail around the origin and hence this point is not shown on the figures. In figure 18, we show the images of the imaginary axis for $\tau = 0.1$ and $m = 8.0, 8.351$ and 8.55. The contour does not enclose the origin when $m = 8.0$. But portions of the contour gradually move to the left as m increases. The transition to instability occurs for $m = 8.351$, at which point, the locus touches the origin. Thereafter, the locus encloses the origin. In fact, at $m = 8.55$, it is evident that there are two enclosures of the origin, signifying two unstable modes. This double enclosure reveals the presence of a complex conjugate pair of eigenvalues that have passed into the right half plane; that is, a Hopf bifurcation has occurred. Note that the loci always pass through the origin for $\lambda = 0$; $D(0) = 0$. This corresponds to the translational invariance of the problem, but this passage through the origin does not lead to an enclosure and is not associated with instability.

The limit when $\tau = 0$ can be similarly treated, the order of the system is reduced by one, and the transition occurs for $m = 7.649$ (with Hopf frequency 0.165); this agrees with results from the direct numerical simulations. There is, however, one fundamental difference in the $\tau = 0$ case, in that the underlying travelling wave solution now has algebraic, and not exponential decay as $\xi \to +\infty$. It is worth noting that, as we have described it, Evans method finds only instabilities that decay exponentially. If $\tau \neq 0$ and the front decays exponentially, then we are guaranteed by arguments mentioned in the main text that this kind of instability is relevant to the initial-value problem. However, instabilities that decay algebraically are not detected. Hence, for $\tau = 0$ and algebraically decaying fronts, it is not guaranteed that the Nyquist theory uncovers the important unstable modes. However numerical solutions to the PDE suggest that the exponentially decaying mode is the important one.

(*a*) *Arrhenius combustion systems*

The related combustion system with Arrhenius exponential terms can be treated in a similar manner. For comparative purposes we calculate the Evans function for this system and determine the stability boundary. The underlying equations

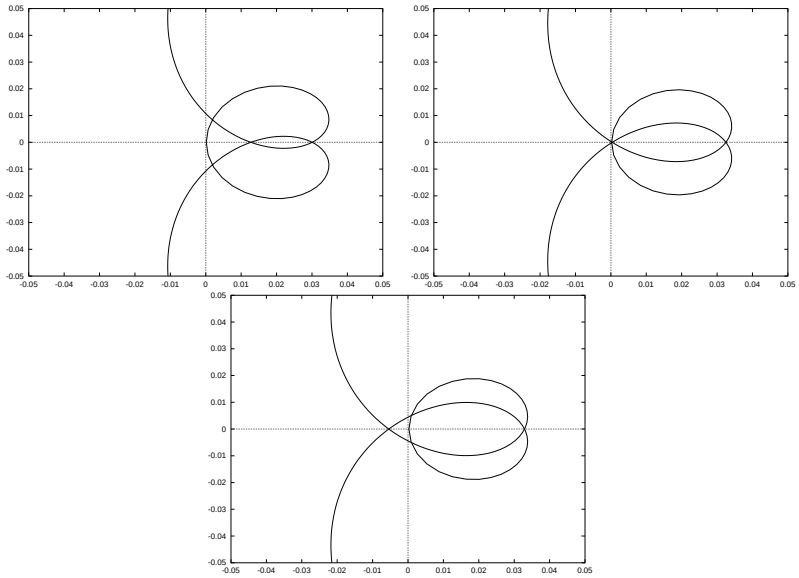

Figure 18. The image of the imaginary axis in the neighbourhood of the origin for $\tau = 0.1$ and, from the top, for $m = 8.0, 8.35$ and 8.55.

in an infinite domain, after rescaling as in Margolis (1991), are

$$u_{xx} + v\Lambda \exp\left(\frac{N(1-\sigma)(u-1)}{\sigma + (1-\sigma)u}\right) = u_t, \tag{A 19}$$

$$\tau v_{xx} - v\Lambda \exp\left(\frac{N(1-\sigma)(u-1)}{\sigma + (1-\sigma)u}\right) = v_t. \tag{A 20}$$

The parameters N and σ are the nondimensionalized activation energy and ratio of unburnt to burnt fuel temperatures, and Λ is the "steady planar flame speed eigenvalue". The autocatalyst u is analogous to the fuel temperature and the reactant v to the fuel concentration. The inverse of the Lewis number is again τ; in many combustion studies, particularly for solid fuels, this is taken to be zero. The other extreme, $\tau = 1$, occurs for combustion in gases.

The boundary conditions are that

$$u \to 1,\ v \to 0 \text{ as } \xi \to -\infty \qquad \text{and} \qquad u \to 0,\ v \to 1 \text{ as } \xi \to \infty. \tag{A 21}$$

In addition, the reaction terms must be cut off to the right of the front; that is, for $u < u^\star$ where $u^\star$ is the "ignition temperature". This is needed to apply boundary conditions at the right of the domain. Here, we take a large domain and cut off the reaction terms far ahead of the front, verifying subsequently that the precise position of the cut-off did not affect any of the results too significantly.

The rescaling implicit in (A 19)-(A 20) absorbs the steady planar flame speed into the eigenvalue, Λ, leaving the rescaled front speed as unity. Thus steadily propagating solutions are given by $u(x-t)$ and $v(x-t)$. The eigenvalue, Λ is unknown and is determined numerically using shooting.

Linearizing as in (A 1), except that now $\xi = x - t$, the coupled evolution

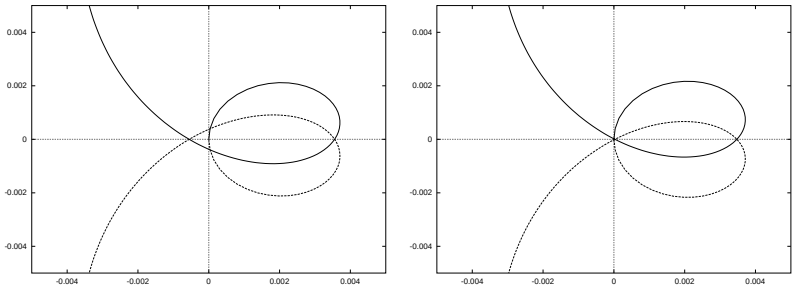

Figure 19. The image of the imaginary axis in the neighbourhood of the origin for $\tau = 0.0$ and for $N = 30$ and $\mu = 4.236$ (left) and $\mu = 4.18$ (right).

equations for the perturbations are

$$\psi_{1t} = \psi_{1\xi\xi} + V\Lambda\psi_1 \exp\left(\frac{N(1-\sigma)(U-1)}{\sigma+(1-\sigma)U}\right)\frac{N(1-\sigma)}{(\sigma+(1-\sigma)U)^2}$$

$$+\Lambda\psi_2 \exp\left(\frac{N(1-\sigma)(U-1)}{\sigma+(1-\sigma)U}\right) + \psi_{1\xi}, \qquad (A\,22)$$

$$\psi_{2t} = \tau\psi_{2\xi\xi} - V\Lambda\psi_1 \exp\left(\frac{N(1-\sigma)(U-1)}{\sigma+(1-\sigma)U}\right)\frac{N(1-\sigma)}{(\sigma+(1-\sigma)U)^2}$$

$$-\Lambda\psi_2 \exp\left(\frac{N(1-\sigma)(U-1)}{\sigma+(1-\sigma)U}\right) + \psi_{2\xi}. \qquad (A\,23)$$

Once the reaction terms are cut off far ahead of the front, then the analogous matrix operator to A (A 5) has the same limits at $\xi \to \pm\infty$. Hence the eigenfunctions have the same growth and decay behaviour at infinity and the analysis required to define the Evans function is identical; the only difference is in the computation of the transmission coefficients.

Following Bayliss & Matkowsky (1990) we define another parameter, $\mu = N(1-\sigma)/2$, and use this in presenting the results. In figure 19, Nyquist plots for $\mu = 2+\sqrt{5} \sim 4.236$ and $\mu = 4.18$ are shown, with $N = 30$ and $\tau = 0$. For $\mu = 2+\sqrt{5}$ the Nyquist plot encloses the origin twice, indicating a complex conjugate pair of unstable modes; the existence of instability at these parameter values is borne out by a full numerical simulation of the PDE. For $\mu \simeq 4.18$, the curves pass through the origin, signifying the marginally stable state. This value is consistent with the results of Bayliss & Matkowsky (1990) who present figures implying a Hopf bifurcation somewhere in the range $3.975 < \mu < 4.425$.

For fixed N, and varying τ we find the neutral stability boundaries shown in figure 20. These marginally stable values of μ alter slightly if the position at which the reaction terms are cut off is varied. Note that the critical value of μ is $2+\sqrt{5}$ at $\tau = 0$ for analytically tractable models using delta-function reaction terms Matkowsky & Sivashinsky (1978).

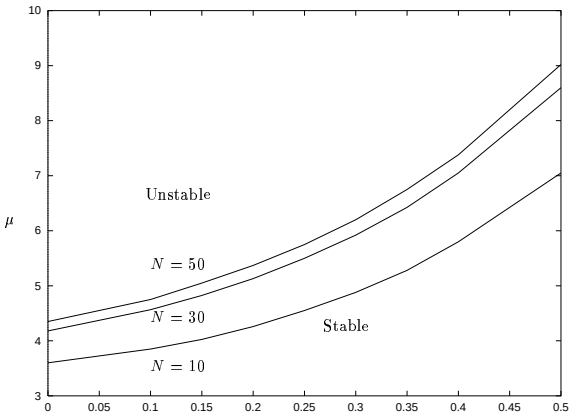

Figure 20. The neutral stability boundary, $\mu = \mu(\tau, N)$, on the $(\tau, \mu)-$plane for $N = 10$, 30 and 50.

Appendix B. Matched asymptotic expansion

In this appendix, we show how the autocatalytic system can be placed into a form for which the derivation of the $m \gg 1$ matched asymptotic expansion proceeds as for combustion systems with Arrhenius kinetics.

First we define a small parameter: $\epsilon = m^{-1}$. Next, we consider the frontal solution in the form,

$$u = u(x - \epsilon\tilde{c}t - \phi, \epsilon^2 t) =: u(\xi, T) \qquad \text{and} \qquad v = v(x - \epsilon\tilde{c}t - \phi, \epsilon^2 t) =: v(\xi, T), \tag{B 1}$$

where $\phi(\epsilon^2 t)$ denotes the position of the front in a frame moving the speed of the equilibrium front, $c = \epsilon\tilde{c}$. Note that the rescaling of the front speed, $c = \epsilon\tilde{c}$, is consistent with the numerical results displayed in figure 2. In the moving frame, the fields and the front position are assumed to depend on the slower timescale $T = \epsilon^2 t$. This is again consistent with numerical calculations, which show that the Hopf frequency becomes very small as τ, and hence $m_c(\tau)$, become larger (see figure 3).

With the definitions in (B 1), we may rewrite the governing equations like so:

$$u_{\xi\xi} + u^m v = -\epsilon\tilde{c}u_\xi + \epsilon^2(\phi_T u_\xi + u_T) \tag{B 2}$$

and

$$\tau v_{\xi\xi} - u^m v = -\epsilon\tilde{c}v_\xi + \epsilon^2(\phi_T v_\xi + v_T). \tag{B 3}$$

The next step is to rewrite the reaction term to bring out its asymptotic form. This term has the factor u^m. Since $m \gg 1$, wherever u is less than unity, the term is therefore likely to be negligibly small. Let

$$u = 1 - \epsilon\theta \qquad \text{and} \qquad v = \epsilon y. \tag{B 4}$$

Then the reaction term becomes

$$u^m v = \epsilon(1-\epsilon\theta)^m y \equiv \epsilon y e^{m\log(1-\epsilon\theta)} = \epsilon y e^{-\theta}\left(1-\frac{1}{2}\epsilon\theta^2+\ldots\right). \tag{B 5}$$

Thus, except for regions in which u is $O(\epsilon)$ less than unity, the reaction term is exponentially small.

The region in which $u = 1 - O(\epsilon)$ lies to the left in the moving coordinate frame. Here v is also order ϵ, which motivates the second relation in (B 4). This is the "inner region", with dependent variables θ and y. In terms of these variables, the inner equations are

$$\theta_{\xi\xi} - y e^{-\theta} = -\epsilon\tilde{c}\theta_\xi + \epsilon^2\left(\phi_T\theta_\xi + \theta_T - \frac{1}{2}y\theta^2 e^{-\theta}\right) \tag{B 6}$$

and

$$\tau y_{\xi\xi} - y e^{-\theta} = -\epsilon\tilde{c}y_\xi + \epsilon^2\left(\phi_T y_\xi + y_T - \frac{1}{2}y\theta^2 e^{-\theta}\right). \tag{B 7}$$

The boundary conditions at the left-hand side of the domain may be directly applied to the inner solution: $u \to 1$ and $v \to 0$ as $\xi \to -\infty$, which translates to $\theta, y \to 0$.

The leading-order terms in (B 6)-(B 7) indicate that inside the inner region, the dominant balance is between the reaction and diffusion terms alone; the convection terms and time derivatives lie at higher order. The inner region terminates as ξ increases and θ grows to order one values. Then, u becomes significantly less than unity and the reaction terms disappear completely from the problem, requiring another dominant balance amongst the terms in the equations. This balance is achieved in the "outer region".

For the outer region, we return to (B 2)-(B 3), and rescale the spatial coordinate: $X = \epsilon\xi$. Then,

$$u_{XX} + \tilde{c}u_X + u_T = \epsilon\phi_T u_X \tag{B 8}$$

and

$$\tau v_{XX} + \tilde{c}v_X + v_T = \epsilon\phi_T v_X. \tag{B 9}$$

These are the outer equations to which we apply the right-hand boundary conditions, $u \to 0$ and $v \to 1$ as $X \to \infty$.

Thus the asymptotic prescription is to solve the inner equations in the left-hand part of the domain on an order one lengthscale, and the outer equations on a long lengthscale to the right. This structure to the problem is obvious in the numerical solutions for the fronts in figure 1, and the linear eigenfunctions in figure 4.

To find the solutions to the inner and outer equations, we pose the asymptotic sequences,

$$u = u_0 + \epsilon u_1 + \ldots, \quad v = v_0 + \epsilon u_1 + \ldots, \quad \theta = \theta_1 + \epsilon\theta_2 + \ldots \quad \text{and} \quad y = y_1 + \epsilon y_2 + \ldots, \tag{B 10}$$

and solve order by order in ϵ. In line combustion theory we also introduce the expansion of the Lewis number: $\tau = \tau_0 + \epsilon\tau_1 + \ldots$. Also, we must compute $\tilde{c}$ by another sequence: $\tilde{c} = c_1 + \epsilon c_2 + \ldots$ The complete solution is given when we match the inner and outer solutions in an intermediate region.

From hereon, the problem is recognized to be identical to all intensive purposes

with the combustion problem (Fife 1988; Sivashinsky 1977).† We will not repeat the calculation, but only quote the salient results.

At leading order, we emerge with the front shape together with the condition,

$$c_1 = \sqrt{\frac{2}{\tau}}. \tag{B 11}$$

This relation is just the asymptotic front speed quoted in a different way in equation (5.1).

At next order, we obtain the leading-order form of the linear eigenfunction, provided we take a solvability condition that amounts to $\tau_0 = 1$. That is, we expand about a Lewis number of unity. At this stage we also assume the temporal dependence, $e^{\tilde{\lambda}T}$, for this part of the solution.

Finally, at order ϵ^3, matching indicates that

$$\tilde{D}(\tilde{\lambda}) = 2\Gamma^2(\Gamma - 1) - \tau_1(\Gamma - 1 - \tilde{\lambda}) = 0, \tag{B 12}$$

where $\Gamma = \sqrt{1 + 2\tilde{\lambda}}$. This equation provides the eigenvalue of linear stability theory as a function of τ_1. But if we look only for the point of marginally stability, then we find the stability threshold, $\tau_1 = 10.9282$, at which point the frequency is given by $\tilde{\lambda} = 1.2712i$. These lead to equations (5.2) and (5.3).

Note that $\tilde{D}(\tilde{\lambda})$ is related to the asymptotic form of the Evans function (*cf.* Terman 1990).

Appendix C. Exponential Order Proof

In this appendix we prove that if $u(0)$ and $1 - v(0)$ are $\mathcal{O}(e^{-\nu x})$ for large x and some $\nu > 0$, then $u(t)$ and $1 - v(t)$ are $\mathcal{O}(e^{-\nu x})$. With $\mathbf{u} = (u, v)$ we can formulate (2.1,2.2) as follows

$$\partial_t \mathbf{u} + \mathcal{A}\mathbf{u} = \mathbf{N}(\mathbf{u}), \tag{C 1}$$

where $\mathcal{A} = -\mathcal{T}\partial_x^2$ with $\mathcal{T}$ a diagonal matrix with 1 and τ down the leading diagonal, and

$$\mathbf{N}(\mathbf{u}) = \begin{pmatrix} +1 \\ -1 \end{pmatrix} v f(u).$$

Let $\tilde{U}(x)$ and $\tilde{V}(x)$ be smooth stationary profiles satisfying the boundary conditions for the autocatalyst and reactant concentrations respectively. Further suppose that $0 \leq \tilde{U} \leq 1$, $0 \leq \tilde{V} \leq 1$ on $I\!R$ and that $\partial_x \tilde{U}$, $\partial_x \tilde{V}$ and $\tilde{U}\tilde{V}$ have compact support on $I\!R$. Let us assume the linear decompositions $u = \tilde{U} + \hat{u}$ and $v = \tilde{V} + \hat{v}$ (Larrouturou 1988; Malham & Xin 1998) so that $\hat{\mathbf{u}} \to 0$ as $|x| \to \infty$ and (C 1) becomes

$$\partial_t \hat{\mathbf{u}} + \mathcal{A}\hat{\mathbf{u}} = \mathbf{N}(\mathbf{u}) - \mathcal{A}\tilde{\mathbf{U}}, \tag{C 2}$$

† Note that it is often the case that in the combustion literature, two outer regions are posed, with the second lying to the left of the inner region. This is not necessary in the one-dimensional problem; the left-hand outer region is really part of the inner solution.

Now let us define the inner product space $H_{\mathcal{B}}$ with ($\mathbf{u}^T$ is transpose)

$$\langle \mathbf{u}, \mathbf{u}' \rangle_{H_{\mathcal{B}}} = \int_{\boldsymbol{R}} \mathbf{u}^T \mathcal{B} \mathbf{u}' \, \mathrm{d}x$$

where $\mathcal{B}(x)$ is a 2×2 matrix of smooth positive functions chosen so that the norm $\|\mathbf{u}\|^2_{H_{\mathcal{B}}} = \langle \mathbf{u}, \mathbf{u} \rangle_{H_{\mathcal{B}}}$ is positive definite. Consider the inner product of (C 2) with $\hat{\mathbf{u}}$ in $H_{\mathcal{B}}$:

$$\frac{1}{2} \frac{\mathrm{d}}{\mathrm{d}t} \langle \hat{\mathbf{u}}, \hat{\mathbf{u}} \rangle_{H_{\mathcal{B}}} + \langle \hat{\mathbf{u}}, \mathcal{A} \hat{\mathbf{u}} \rangle_{H_{\mathcal{B}}} = \langle \hat{\mathbf{u}}, \mathbf{N}(\mathbf{u}) \rangle_{H_{\mathcal{B}}} - \langle \hat{\mathbf{u}}, \mathcal{A} \tilde{\mathbf{U}} \rangle_{H_{\mathcal{B}}}. \tag{C 3}$$

Integration by parts shows that

$$\langle \hat{\mathbf{u}}, \mathcal{A} \hat{\mathbf{u}} \rangle_{H_{\mathcal{B}}} = \langle \partial_x \hat{\mathbf{u}}, \partial_x \hat{\mathbf{u}} \rangle_{H_{\mathcal{B}\mathcal{T}}} + \int_{\boldsymbol{R}} \hat{\mathbf{u}}^T \partial_x (\mathcal{B}\mathcal{T}) \partial_x \hat{\mathbf{u}} \, \mathrm{d}x. \tag{C 4}$$

We now take $\mathcal{B}$ to have the explicit form:

$$\mathcal{B}(x) = \begin{pmatrix} \alpha & \beta \\ \beta & \gamma \end{pmatrix} \varphi(x),$$

where α, β and γ are positive constants and φ is a positive, smooth, monotonically increasing function that is unity for all $x \leq 0$ and for some $\nu > 0$:

$$\varphi = \exp(\nu x) \text{ for all } x \geq 1 \quad \text{and} \quad |\varphi'(x)| \leq C\varphi(x) \text{ for all } x \geq 0. \tag{C 5}$$

Hereafter C will denote a generic finite constant which could depend on any of the parameters mentioned thus far. The following estimate for that last term in (C 4) is immediate from the Young inequality:

$$\int_{\boldsymbol{R}} \hat{\mathbf{u}}^T \partial_x (\mathcal{B}\mathcal{T}) \partial_x \hat{\mathbf{u}} \, \mathrm{d}x \leq \frac{1}{2} \langle \partial_x \hat{\mathbf{u}}, \partial_x \hat{\mathbf{u}} \rangle_{H_{\mathcal{B}\mathcal{T}}} + C \langle \hat{\mathbf{u}}, \hat{\mathbf{u}} \rangle_{H_{\mathcal{B}}}. \tag{C 6}$$

Similarly the Young inequality reveals that

$$\langle \hat{\mathbf{u}}, \mathcal{A} \tilde{\mathbf{U}} \rangle_{H_{\mathcal{B}}} \leq C \langle \hat{\mathbf{u}}, \hat{\mathbf{u}} \rangle_{H_{\mathcal{B}}} + C \langle \partial_x^2 \tilde{\mathbf{U}}, \partial_x^2 \tilde{\mathbf{U}} \rangle_{H_{\mathcal{B}}}, \tag{C 7}$$

where the last term is bounded by a constant C as $\partial_x^2 \tilde{\mathbf{U}}$ has compact support. Finally we can estimate the nonlinear term as follows

$$\langle \hat{\mathbf{u}}, \mathbf{N}(\mathbf{u}) \rangle_{H_{\mathcal{B}}} = - \int_{\boldsymbol{R}} [(\beta - \alpha)\hat{u} + (\gamma - \beta)\hat{v}] v f(u) \varphi(x) \, \mathrm{d}x \leq C \langle \hat{\mathbf{u}}, \hat{\mathbf{u}} \rangle_{H_{\mathcal{B}}}, \tag{C 8}$$

where we have assumed that $\beta - \alpha > 0$ and $\gamma - \beta > 0$ so that for $\hat{u}$ sufficiently large in (C 8) the integral on the left-hand side is in fact negative and therefore we are merely concerned with $\hat{u} \leq$ large constant. Note that for arbitrary $\varepsilon > 0$ and $\delta > 0$ the Young inequality guarantees that

$$\hat{\mathbf{u}}^T \mathcal{B} \hat{\mathbf{u}} \geq (\alpha - \beta\varepsilon)\hat{u}^2 \varphi + (\gamma - \beta/\varepsilon)\hat{v}^2 \varphi$$

and

$$(\partial_x \hat{\mathbf{u}})^T (\mathcal{B}\mathcal{T}) (\partial_x \hat{\mathbf{u}}) \geq (\alpha - (1+\tau)\beta\delta) |\partial_x \hat{u}|^2 \varphi + (\tau\gamma - (1+\tau)\beta/\delta) |\partial_x \hat{v}|^2 \varphi.$$

Therefore given $\alpha > 0$, we can choose β, ε, δ and finally γ so that: $\beta - \alpha > 0$; $\langle \hat{\mathbf{u}}, \hat{\mathbf{u}} \rangle_{H_{\mathcal{B}}}$ is equivalent to a weighted L^2-norm with weight φ; $\langle \partial_x \hat{\mathbf{u}}, \partial_x \hat{\mathbf{u}} \rangle_{H_{\mathcal{B}\mathcal{T}}} \geq 0$ and $\gamma - \beta > 0$. Combining (C 3)–(C 8) we see that

$$\frac{\mathrm{d}}{\mathrm{d}t} \langle \hat{\mathbf{u}}, \hat{\mathbf{u}} \rangle_{H_{\mathcal{B}}} + \langle \partial_x \hat{\mathbf{u}}, \partial_x \hat{\mathbf{u}} \rangle_{H_{\mathcal{B}\mathcal{T}}} \leq C \langle \hat{\mathbf{u}}, \hat{\mathbf{u}} \rangle_{H_{\mathcal{B}}} + C. \tag{C 9}$$

and therefore applying the Gronwall inequality reveals that $\langle \hat{\mathbf{u}}, \hat{\mathbf{u}} \rangle_{H_B}$ grows at worst exponentially in time and the result follows.

Appendix D. Two–dimensional stability

Linear stability results for the two–dimensional problem are presented here; we consider both $\tau > 1$ and $\tau < 1$. For $\tau < 1$ it is conceivable that perturbations in the transverse direction could substantially alter the marginal stability curves leading to more readily obtainable values of m. For $\tau > 1$, Horváth *et al.* (1993) and Zhang & Falle (1994) have previously considered coupled cubic and quadratic autocatalysis and shown the existence of an instability that is unrelated to any one-dimensional one.

For the two-dimensional problem, the governing equations are

$$u_t = u_{xx} + u_{yy} + v f(u) \tag{D 1}$$

and

$$v_t = \tau(v_{xx} + v_{yy}) - v f(u). \tag{D 2}$$

The function $f(u)$ is defined in (2.3). We consider these equations in the infinite domain, $-\infty < x < \infty$ and $-L \le y \le L$, with the boundary conditions that

$$u(x, y, t) \to 1, \ v(x, y, t) \to 0 \text{ as } x \to -\infty \tag{D 3}$$

$$\text{and } u(x, y, t) \to 0, \ v(x, y, t) \to 1 \text{ as } x \to \infty, \tag{D 4}$$

We take either periodic boundary conditions in y, $u(x, -L, t) = u(x, L, t)$ and $v(x, -L, t) = v(x, L, t)$ or no flux conditions, $u_y(x, -L, t) = u_y(x, L, t) = 0$ and $v_y(x, -L, t) = v_y(x, L, t) = 0$.

These equations have solutions in the form of planar, steadily propagating fronts of the form, $U = U(\xi) = U(x - ct)$ and $V = V(\xi) = V(x - ct)$, and which are identical in cross-section to the one-dimensional fronts considered in the main text. In this Appendix, we will consider only the linear stability of these fronts.

As in Appendix A we consider infinitesimal perturbations of the form,

$$\psi_j(\xi, y, t) = \hat{\psi}_j(\xi, t) F(y) \quad \text{for} \quad j = 1, 2, \tag{D 5}$$

where we include dependence on the coordinate y through the function $F(y)$, satisfying $F'' + k^2 F = 0$ and the appropriate boundary conditions. For periodic domains $F = e^{iky}$, and for no-flux boundaries, $F = \cos ky$. with $k = 2n\pi/L$.

The linear stability problem is then again given by (A 4), but now with the operator

$$A = \begin{pmatrix} \partial_\xi^2 - k^2 + mU^{m-1}V + c\partial_\xi & U^m \\ -mU^{m-1}V & \tau(\partial_\xi^2 - k^2) - U^m + c\partial_\xi \end{pmatrix}, \tag{D 6}$$

which contains k^2 as an additional parameter.

Both the Newton–Raphson–Kantorovich scheme and the Evans function analysis can be used to solve this system. For the Evans functions, the analysis is identical; the additional terms proportional to k^2 do not change the structure of the calculation. The transmission functions $d_j(\lambda, k^2)$ are determined using the same complementary problems, and lead to an Evans function, $D(\lambda, k^2)$.

The stability boundaries are now given by $m = m_c(\tau, k)$. Since k appears as an

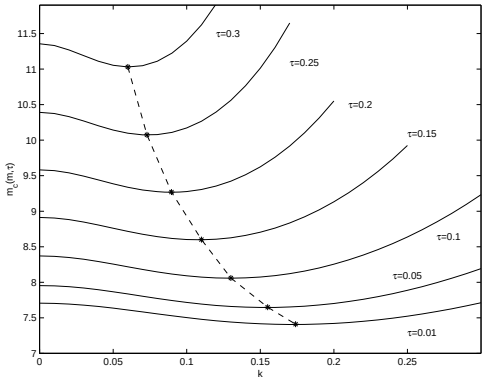

Figure 21. The stability boundaries, $m = m_c(\tau, k)$, are shown drawn on the $(k, m)-$plane for $\tau < 1$. The stability boundaries take their minimal values at finite wavenumber indicating that the points of marginal stability do not occur at $k = 0$. The dashed line shows the locus of the minima, which gives the points of marginal stability, $m = m_*(\tau)$ and $k = k_*(\tau)$.

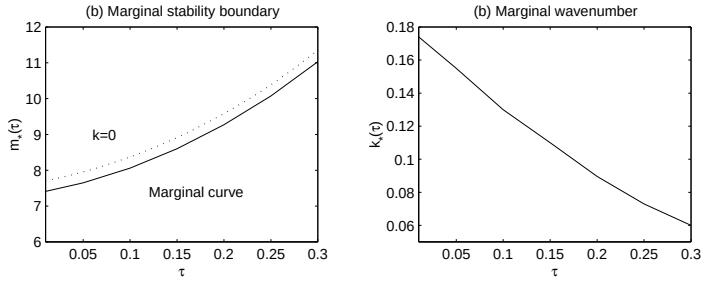

Figure 22. The points of marginal stability, $m = m_*(\tau)$ and $k = k_*(\tau)$. In (a), the one-dimensional ($k = 0$) result is also shown for comparison.

additional parameter, we must vary k over its possible range of values in order to find the smallest possible value for m_c that gives instability. This defines the point of marginal stability, $m = m_*(\tau)$ and $k = k_*(\tau)$, as a function of τ.

Stability boundaries for $\tau < 1$ are illustrated in figure 21. These boundaries are displayed on the $m_c(\tau, k)-$plane for different values of τ. Evidently instability sets in first at finite transverse wavenumber, but as shown in figure 22, the point of marginal stability, $m = m_*(\tau)$, is little different from the one-dimensional stability boundary, $m = m_c(\tau, 0)$. Hence, even in two dimensions, the instability sets in at rather large values of m.

Nyquist plots for $\tau = 0.2$ and $m = 9.267$ are shown in figure 23. For these values of τ and m, the Nyquist curves never enclose the origin. However, for the two cases shown in the figure, the curve passes through the origin. At $k = 0$, the passage of the curve through the origin reflects a point of neutral stability associated with translational invariance: $D(0, 0) = 0$. For slightly larger k, translational symmetry is broken, and the Nyquist curves pass to the left of the origin. However, at larger k, the curve passes once again through the origin ($k \approx 0.0896$). This corresponds to the point of marginal stability for $\tau = 0.2$.

As remarked above, when $\tau > 1$, the linear stability of planar fronts is completely different from the one-dimensional version: whereas the one-dimensional system appears to be always stable in this parameter regime, we observe transitions to instability for planar fronts (see figure 24). These instabilities are direct

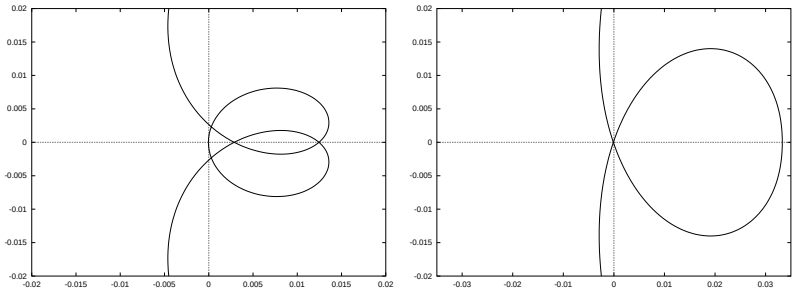

Figure 23. Nyquist plots (the image of the imaginary axis, $D(iy, k^2)$ for $-\infty < y < \infty$), in the neighbourhood of the origin for $m = 9.267$, $\tau = 0.2$ and $k = 0$ and 0.0896.

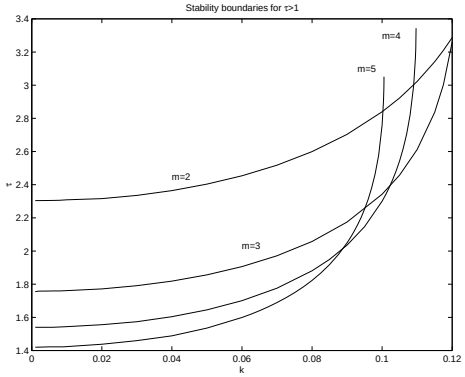

Figure 24. Stability boundaries, $m = m_c(\tau, k)$, for $\tau > 1$. The boundaries are shown on the $(k, \tau)-$plane for different values of m. Specifically, $m = 2, 3, 4$ and 5 are shown. The points of marginal stability occur at $k = 0$, although $k = 0$ is itself never unstable (by translational symmetry it must be neutrally stable).

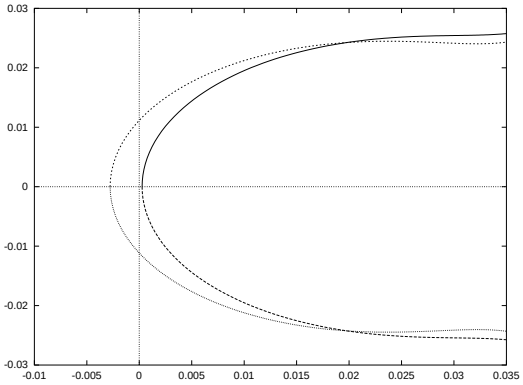

Figure 25. Nyquist plots (the image of the imaginary axis, $D(iy, k^2)$, for $-\infty < y < \infty$) in the neighbourhood of the origin for $m = 5$ and $\tau = 2.5$; the solid line is for $k = 0.1$ and the dashed line for $k = 0.08$.

instabilities that lead to corrugations in the front position. Hence they emerge as single enclosures in the Nyquist plots, see figure 25. These instabilities are explored by Horváth *et al.* (1993) and Malevnets *et al.* (1996).

The instabilities indicated in figures 21-25 continue to exist for large m, though the stability boundaries recede to small k and $\tau = 1$. This can be verified by

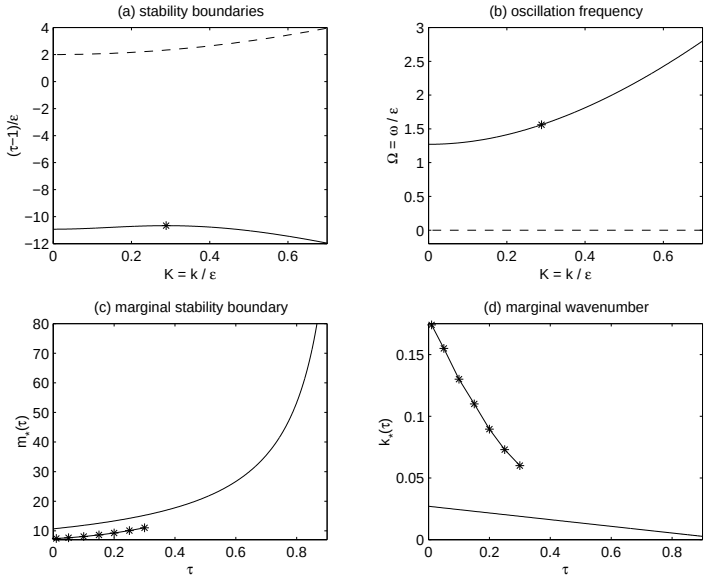

Figure 26. Stability boundaries for the asymptotic result in (D 7). Panel (a) shows the stability boundary $(\tau-1)/\epsilon$ against $K = k/\epsilon$, and (b) shows the associated oscillation (Hopf) frequencies, $\Omega = \omega/\epsilon^2 = -i\lambda/\epsilon^2$. Oscillatory instability is shown by solid lines, direct instability as the dashed line. The star indicates the point of marginal stability for $\tau < 1$ in the scaled variables, $(\tau-1)/\epsilon$ and $K = k/\epsilon$. By removing the asymptotic scaling we arrive at the unscaled points of marginal stability which are displayed in panels (c) and (d), where they are compared with the numerical results.

performing a matched asymptotic expansion as in Appendix B. The analysis is again identical to that used in the combustion problem at high activation energy. The calculation is not very different and again leads to

$$\tilde{D}(\tilde{\lambda}) = 2\Gamma^2(\Gamma - 1) - \tau_1(\Gamma - 1 - \tilde{\lambda}) = 0, \qquad \text{(D 7)}$$

but with $\Gamma = \sqrt{1 + 2\tilde{\lambda} + 2K^2}$, where $K = k/\epsilon$. The asymptotic stability boundary is shown in figure 26 where it is compared with numerical results.

References

Aldushin, A. P., Martemyanova, T. M., Merzhanov, A. G., Khalin, B. I. & Shkadinskii, K. G., 1975. Autovibrational propagation of the combustion front in heterogeneous condensed media. *Combustion, Explosion and Shock Waves* **9**, 531–542.

Alexander, J., Gardner, R. & Jones, C., 1990. A topological invariant arising in the stability analysis of travelling waves. *J. reine angew. Math.* **410**, 167–212.

Bayliss, A. & Matkowsky, B. J., 1990. Two routes to chaos in condensed phase combustion. *SIAM J. Appl. Maths* **50**, 437–459.

Bayliss, A., Matkowsky, B. J. & Minkoff, M., 1989. Period doubling gained, period doubling lost. *SIAM J. Appl. Maths* **49**, 1047–1063.

Berestycki, H., Nicolaenko, B. & Scheurer, B., 1985. Travelling wave solutions to combustion models and their singular limits. *SIAM J. Math. Anal.* **16**, 1207–1242.

Billingham, J. & Needham, D. J., 1991. The development of travelling waves in quadratic and cubic autocatalysis with unequal diffusion rates. I. Permanent form of travelling waves. *Phil. Trans. R. Soc. Lond. A* **334**, 1–24.

Blom, J. G. & Zegeling, P. A., 1994. Algorithm 731: a moving-grid interface for systems of one-dimensional time-dependent partial differential equations. *ACM Trans. Math. Software* **20**, 194–214.

Bonnet, A., Larrouturou, B. & Sainsaulieu, L., 1993. On the stability of multiple steady planar flames when the Lewis number is less than 1. *Physica D* **69**, 345–352.

Cash, J. R. & Singhal, A., 1982. High order method for the numerical solution of two-point boundary value problems. *BIT* **22**, 184–188.

Elezgaray, J. & Arneodo, A., 1991. Modelling reaction-diffusion pattern formation in the Couette flow reactor. *J. Chem. Phys.* **95**, 323–350.

Evans, J. W., 1975. Nerve axon equations, IV: the stable and unstable impulse. *Indiana Univ. Math. J.* **24**, 1169–1190.

Fife, P. C., 1988. *Dynamics of internal layers and diffusive interfaces.* CBMS-NSF Regional conference series in Applied Mathematics.

Henry, D., 1981. *Geometric Theory of Semilinear Parabolic Equations.* Springer-Verlag.

Horváth, D., Petrov, V., Scott, S. K. & Showalter, K., 1993. Instabilities in propagating reaction-diffusion fronts. *J. Chem. Phys.* **98**, 6332–6343.

Ikeda, T. & Mimura, M., 1993. An interfacial approach to regional segregation of two competing species mediated by a predator. *J. Math.Biol.* **31**, 215–240.

Keast, P. & Muir, P. H., 1991. Algorithm 688 EPDCOL - a more efficient PDECOL code. *ACM Trans. Math. Software* **17**, 153–166.

Langer, J. S., 1980. Instabilities and pattern formation in crystal growth. *Rev. Mod. Phys.* **52**, 1–28.

Larrouturou, B., 1988. The equations of one-dimensional unsteady flame propagation: existence and uniqueness. *SIAM J. Math. Anal.* **19**, 32–59.

Malevanets, A., Careta, A. & Kapral, R., 1996. Biscale chaos in propagating fronts. *Phys. Rev. E* **52**, 4724–4735.

Malham, S. J. A. & Xin, J., 1998. Global solutions to a reactive Boussinesq system with front data on an infinite domain. To appear in CMP.

Margolis, S. B., 1991. The transition to nonsteady deflagration in gasless combustion. *Prog, Energy Combust. Sci.* **17**, 135–162.

Matkowsky, B. J. & Sivashinsky, G. I., 1978. Propagation of a pulsating reaction front in solid fuel combustion. *SIAM J. Appl. Maths.* **35**, 465–478.

Metcalf, M. J., Merkin, J. H. & Scott, S. K., 1994. Oscillating wave fronts in isothermal chemical systems with arbitrary powers of autocatalysis. *Proc. Roy. Soc. Lond. A* **447**, 155–174.

Nagypal, I. & Epstein, I., 1988. Stochastic behaviour and stirring rate effects in the chlorite-iodide reaction. *J. Chem. Phys.* **89**, 6925–6928.

Nishiura, Y. & Mimura, M., 1989. Layer oscillations in reaction-diffusion systems. *SIAM J. Appl. Math.* **49**, 482–514.

PEGO, R. L., SMEREKA, P. & WEINSTEIN, M. I., 1993. Oscillatory instability of traveling waves for a KdV-Burgers equation. *Physica D* **67**, 45–65.

PEGO, R. L. & WEINSTEIN, M. I., 1992. Eigenvalues and instabilities of solitary waves. *Phil. Trans. Roy. Soc. Lond. A* **340**, 47–94.

SHKADINSKII, K. G., KHALIN, B. I. & MERZHANOV, A. G., 1973. Propagation of a pulsating exothermic reaction front in the condensed phase. *Combustion, Explosion and Shock Waves* **1**, 15–22.

SIVASHINSKY, G. I., 1977. Diffusional-thermal theory of cellular flames. *Comb. Sci. Tech.* **15**, 137–146.

SOLOVYOV, S. E., ILYASHENKO, V. M. & POJMAN, J. A., 1997. Numerical modelling of self-propagating polymerization fronts: The role of kinetics on front stability. *Chaos* **7**, 331–340.

SWINTON, J. & ELGIN, J., 1990. Stability of travelling pulse solutions to a laser equation. *Phys. Lett. A* **145**, 428–433.

TERMAN, D., 1990. Stability of planar wave solutions to a combustion model. *SIAM J. Math. Anal.* **21**, 1139–1171.

ZHANG, Z. & FALLE, S. A. E. G., 1994. Stability of reaction-diffusion fronts. *Proc. Roy. Soc. Lond. A* **446**, 517–528.